

Simultaneous retrieval of oceanic and atmospheric parameters for ocean color imagery by spectral optimization: a validation

Roman M. Chomko^a, Howard R. Gordon^{a,*}, Stephane Maritorena^b, David A. Siegel^{b,c}

^aDepartment of Physics, University of Miami, P.O. Box 248046, Coral Gables, FL 33124 0530, USA

^bInstitute for Computational Earth System Science, University of California, Santa Barbara, Santa Barbara, CA 93106, USA

^cDepartment of Geography, University of California, Santa Barbara, Santa Barbara, CA 93106, USA

Received 14 February 2002; received in revised form 17 June 2002; accepted 27 June 2002

Abstract

We report application and validation of a spectral optimization algorithm for processing SeaWiFS data in Case 1 waters. The algorithm couples a simplified aerosol model with a sophisticated water-reflectance model to simultaneously retrieve both atmospheric and ocean parameters. Two of the retrieved ocean properties—the absorption coefficient of colored detrital material and the chlorophyll *a* concentration—are validated by comparison with “surface” truth obtained with airborne and space-borne sensors. We show that employing a more complete water reflectance model significantly improves the decoupling between the oceanic and atmospheric optical signals. Methodologies for applying the algorithm to Case 2 waters and for delineating terrestrial vs. marine chromophoric dissolved organic matter (CDOM) are suggested.

© 2002 Elsevier Science Inc. All rights reserved.

1. Introduction

Traditionally, ocean color imagery has been processed in two sequential steps (e.g., Gordon & Morel, 1983). First, an atmospheric correction algorithm is applied to remove the effects of the atmosphere and enable retrieval of the water-leaving reflectance (ρ_w) from the satellite-measured reflectance of the ocean–atmosphere system (ρ_t). Then, the water-leaving reflectances are used in a bio-optical algorithm to extract the chlorophyll concentration associated with phytoplankton in the surface waters. In the case of SeaWiFS (Hooker, Esaias, Feldman, Gregg, & McClain, 1992), the Gordon and Wang (1994) atmospheric correction procedure is applied and the chlorophyll concentration is retrieved from ρ_w using bio-optical algorithms such as described by O’Reilly et al. (1998). A main problem with this approach is accounting for absorbing aerosol effects. The Gordon and Wang (1994) algorithm uses spectral bands in the near infrared (NIR), where $\rho_w \approx 0$, to assess the aerosol’s contribution to the reflectance in the visible. This approach is applicable only for a non- or weakly absorbing aerosol (Gordon, 1997). When the aerosol is strongly absorbing,

associated with both soot or dust aerosols, the NIR reflectance provides no clue to the visible reflectance. This means that the two-step process will fail in the presence of strongly absorbing aerosols, so the visible bands must be used to assess the aerosol absorption. Employing the visible bands, where $\rho_w \neq 0$, requires coupling the ocean property retrieval and the atmospheric correction.

Such coupled algorithms for retrieval of the chlorophyll concentration date back to the proof-of-concept Coastal Zone Color Scanner mission (CZCS, Hovis et al., 1980). The CZCS lacked spectral bands in the NIR, the longest wavelength usable channel being at 670 nm. The initial CZCS algorithms (Gordon, Clark, Mueller, & Hovis, 1980) assumed that the water-leaving reflectance at 670 nm in Case 1 waters was null at all trophic levels. Case 1 waters are defined to be those for which the optical properties are determined by the water itself and phytoplankton along with their immediate detrital material (Gordon & Morel, 1983). Most of the world oceans are Case 1 waters, the remaining are called Case 2 waters, comprising, for example, coastal waters subject to riverine input, resuspended sediments from the bottom, etc. This assumption allowed assessment of the atmospheric effects at 670 nm, leading to an atmospheric correction. However, at even mesotrophic chlorophyll concentrations, the water-leaving reflectance is already detectable in the NIR (Siegel, Wang, Maritorena, & Robinson,

* Corresponding author. Tel.: +1-305-284-2323; fax: +1-305-284-4222.
E-mail address: hgordon@miami.edu (H.R. Gordon).

2000) and is even larger in the red. Thus, in general, the CZCS had no band that was free of ρ_w , and therefore algorithms that coupled ocean property retrieval and atmospheric correction were developed to overcome this difficulty. Some algorithms used empirical relationships between the water-leaving reflectance in the four CZCS visible bands (Smith & Wilson, 1981); others used semi-analytic models relating the four water-leaving reflectances to the phytoplankton pigment concentration (Andre & Morel, 1991; Bricaud & Morel, 1987). All solved the resulting set of nonlinear equations using iterative techniques. SeaWiFS was designed to overcome this difficulty with the addition of spectral bands in the NIR; however, similar techniques are still required for sediment-dominated (Case 2) coastal waters or eutrophic Case 1 waters in which the water-leaving reflectance even in the NIR cannot be ignored (Ruddick, Ovidio, & Rijkeboer, 2000; Siegel et al., 2000).

Several recent attempts have been made to develop coupled ocean–atmosphere correction algorithms for retrieving ocean and aerosol properties through an atmosphere characterized by absorbing aerosols (Chomko & Gordon, 1998; Gordon, Du, & Zhang, 1997). These coupled algorithms use bio-optical models relating the ρ_w to the water's constituents and aerosol models (particle size frequency distribution and complex refractive index) relating the aerosol's contribution to ρ_t as a function of its concentration. Retrieval of the oceanic and atmospheric parameters is then effected by finding the combination of parameter values and an aerosol model that best reproduce the measured ρ_t throughout the spectrum.

Moulin, Gordon, Chomko, Banzon, and Evans (2001) adapted the Gordon et al. (1997) spectral-matching algorithm to effect atmospheric correction of SeaWiFS imagery in the presence of Saharan dust off the coast of West Africa. To implement the algorithm, they used SeaWiFS to develop aerosol models specifically tuned to capture the spectral variation of the dust's contribution to ρ_t (Moulin, Gordon, Banzon, & Evans, 2001). This was necessary because (unlike most aerosols) Saharan dust absorption is a strong function of wavelength—increasing dramatically from red to blue—requiring the imaginary part of the particle refractive index (the absorption index) to be wavelength-dependent. They showed that successful atmospheric correction was possible under conditions when the optical thickness of the dust was as high as 0.8.

Chomko and Gordon (2001) reported the successful operation of a spectral optimization algorithm (SOA, Chomko & Gordon, 1998) for simultaneous atmospheric correction and retrieval of water properties from SeaWiFS imagery. In this algorithm, no effort was made to precisely model the aerosol. Rather, a simple one-parameter Junge-distributed collection of spherical particles was used for the size–shape distribution, along with a wavelength-independent complex refractive index. Such an aerosol model should be adequate for atmospheric correction when the aerosol is non-absorbing or when the absorption index is independent

of wavelength, e.g., black carbon. Application to imagery off the US East Coast showed consistent retrieved water properties between days with turbid and clear atmospheres. However, aerosol properties (particularly the aerosol single scattering albedo) were not well retrieved in clear atmospheres, presumably because large variations in aerosol properties produced only small changes in ρ_t at low aerosol concentration. Unfortunately, because the bio-optical model differed considerably from that for the standard SeaWiFS processing, an unbiased comparison of the SOA and SeaWiFS ocean products was not possible.

Both of these above implementations of coupled ocean–atmosphere algorithms used the Gordon et al. (1988) two-parameter radiance model to provide the oceanic reflectance. The Gordon et al. model expresses the water-leaving radiance as a function of the pigment concentration P and a scattering parameter. However, more complete radiance models are now available (Carder, Chen, Lee, Haws, & Kamykowski, 1999; Garver & Siegel, 1997; Maritorena, Siegel, & Peterson, 2002). These models make it possible to obtain ocean parameters in addition to the chlorophyll a concentration such as particulate backscatter and the absorption by colored dissolved and detrital particulate materials (CDM). In this paper, we combine a globally tuned version of the Garver and Siegel (1997) bio-optical model (Maritorena et al., 2002; hereafter referred to as GSM01) with an improved version of the Chomko and Gordon (1998) SOA. This will enable us to retrieve a set of ocean parameters along with estimates of aerosol optical properties. The ocean retrievals are validated using a combination of airborne laser fluorescence transect observations and SeaWiFS operational products. Comparison of the SOA retrievals with the laser fluorescence estimates of CDM suggests a path by which terrestrial vs. marine dissolved materials may be distinguished with the next generation of ocean color satellite imagery. In addition, we show that the difficulty in retrieving aerosol properties in relatively clear atmospheres is minimized using the GSM01 bio-optical algorithm.

We begin by briefly reviewing radiative transfer, the aerosol models, and the bio-optical model. Next, we describe the mechanics of the spectral optimization algorithm, and validate its retrieval of water properties. Finally, we show that the retrieved aerosol properties are almost completely decoupled from the ocean properties in both clear and turbid atmospheres.

2. Radiative transfer

The reflectance $\rho_t(\lambda)$ of the ocean–atmosphere system at a wavelength λ can be expressed as

$$\rho_t(\lambda) = \rho_r(\lambda) + \rho_A(\lambda) + t_v(\lambda)t_s(\lambda)\rho_w(\lambda), \quad (1)$$

where $\rho_r(\lambda)$ is the pure Rayleigh scattering contribution, $\rho_A(\lambda)$ is the aerosol contribution (in the presence of Rayleigh

scattering), and $\rho_w(\lambda)$ is the normalized water-leaving reflectance. The quantities $t_s(\lambda)$ and $t_v(\lambda)$ are the diffuse transmittances of the atmosphere from the sun to the sea surface and from the sensor to the sea surface, respectively. The atmospheric contribution $\rho_r(\lambda) + \rho_A(\lambda)$ includes light specularly reflected from the sea surface as well as scattered in the atmosphere. All of the information regarding the water's constituents resides in $\rho_w(\lambda)$. Note that we have simplified the earlier notation wherein $\rho_w(\lambda)$ was written $[\rho_w(\lambda)]_N$ (Gordon, 1997), and $\rho_A(\lambda)$ was written $\rho_a(\lambda) + \rho_{ra}(\lambda)$, where $\rho_a(\lambda)$ is the reflectance contribution from aerosol scattering in the *absence* the Rayleigh scattering by the air, and $\rho_{ra}(\lambda)$ is a correction term resulting from interaction between Rayleigh and aerosol scattering (Gordon and Wang, 1994).

3. The aerosol model

The atmospheric contribution $\rho_r(\lambda) + \rho_A(\lambda)$ is computed from an aerosol model in the following manner. First, $\rho_r(\lambda)$ is computed at all wavelengths using a radiative transfer code in which the aerosol-free atmosphere is bounded by a (flat) Fresnel reflecting ocean that absorbs all photons penetrating the surface. Then the same code is used with a model aerosol uniformly mixed with air from the surface to 2 km to compute $\rho_r(\lambda) + \rho_A(\lambda)$, the atmospheric contribution when $\rho_w(\lambda) = 0$, as a function of the aerosol optical thickness at 865 nm (τ_a). Finally, $\rho_r(\lambda)$ is subtracted from $\rho_r(\lambda) + \rho_A(\lambda)$ to provide $\rho_A(\lambda)$ as a function of τ_a . In the aerosol model, particles are distributed according to a Junge power law:

$$\begin{aligned} \frac{dN}{dD} &= 0, & D < D_0, \\ \frac{dN}{dD} &= \frac{K}{D_1^{v+1}}, & D_0 \leq D \leq D_1, \\ \frac{dN}{dD} &= \frac{K}{D^{v+1}}, & D_1 \leq D \leq D_2, \\ \frac{dN}{dD} &= 0, & D > D_2, \end{aligned} \quad (2)$$

where D is the particle diameter and dN is the number of particles per unit volume in the size interval $D \pm dD/2$. We take $D_0 = 0.06 \mu\text{m}$, $D_1 = 0.20 \mu\text{m}$, and $D_2 = 20 \mu\text{m}$. The optical properties of the aerosol are computed from Mie theory using the above size distribution and the complex index of refraction $m = m_r - m_i$. In the present application, m_r is either 1.50 or 1.333, and $m_i = 0, 0.001, 0.003, 0.010, 0.030, \text{ and } 0.040$. The parameter v ranges from 2.0 to 4.5 in steps of 0.5. Thus, there are 72 separate aerosol models (2 values of $m_r \times 6$ values of $m_i \times 6$ values of v). For each of these models, $\rho_A(\lambda)$ is computed as a function of the aerosol

optical thickness $\tau(\lambda)$ for a wide range of viewing and solar geometries and fit to a quartic expression

$$\begin{aligned} \rho_A(G, \lambda, m_r, m_i, v) &= a(G, \lambda, m_r, m_i, v)\tau(\lambda) \\ &+ b(G, \lambda, m_r, m_i, v)\tau^2(\lambda) \\ &+ c(G, \lambda, m_r, m_i, v)\tau^3(\lambda) \\ &+ d(G, \lambda, m_r, m_i, v)\tau^4(\lambda), \end{aligned} \quad (3)$$

where G indicates a particular geometry. The quantities $a, b, c,$ and d are then stored as lookup tables (LUTs) for use by the optimization procedure. The diffuse transmittances are computed separately by assuming that the in-water upwelling radiance distribution just beneath the surface is uniform (Yang & Gordon, 1997).

4. The bio-optical model

In most ocean reflectance models, the water-leaving reflectance (ρ_w) is provided as a function of the absorption (a) and backscattering (b_b) coefficients. The (spectral) absorption and backscattering coefficients are separated into the constituent components plus that of water: $a(\lambda) = a_w(\lambda) + a_{ph}(\lambda) + a_{dp}(\lambda) + a_{CDOM}(\lambda)$ and $b_b(\lambda) = b_{bw}(\lambda) + b_{bp}(\lambda)$, where the subscripts “w”, “ph”, “dp”, “CDOM”, and “p” refer, respectively, to water, phytoplankton, detrital particles, colored dissolved organic matter, and particles of all kinds. Working with a limited data set, Gordon et al. (1988) related the absorption of all of the components to the pigment concentration. Particle backscattering was also modeled as function of P . Hence, the water-leaving reflectance spectrum depended on a single free parameter, P , which assumes that fixed relationships exist between $a_{ph}(\lambda)$, $a_{dp}(\lambda)$ and $a_{CDOM}(\lambda)$ and P .

Recent models for ocean reflectance provide more information than a simple measure of pigment concentration by retrieving relevant optical properties individually (e.g., Carder et al., 1999; Garver & Siegel, 1997; Hoge & Lyon, 1996; Lee et al., 1994; Roesler & Perry, 1995). These models typically combine $a_{dp}(\lambda) + a_{CDOM}(\lambda)$, due to their similar spectral signatures, to form $a_{cdm}(\lambda) \equiv a_{dp}(\lambda) + a_{CDOM}(\lambda)$ (the absorption coefficient of colored detrital material or CDM). However, the remaining components are retrieved individually. The GSM01 model (Garver & Siegel, 1997; Maritorea et al., 2002) retrieves three parameters: (1) the absorption coefficient of colored detrital matter at 443 nm ($a_{cdm}(443)$); (2) the chlorophyll a concentration C , and (3) the backscattering coefficient of particulate matter at 443 nm ($b_{bp}(443)$). Specifically, the nonwater components are modeled as

$$a_{ph}(\lambda) = C a_{ph}^*(\lambda), \quad (4)$$

$$a_{cdm}(\lambda) = a_{cdm}(443)\exp(-S(\lambda - 443)), \quad (5)$$

$$b_{bp}(\lambda) = b_{bp}(443) (443/\lambda)^n, \quad (6)$$

where $a_{ph}^*(\lambda)$ is the chlorophyll specific absorption coefficient spectrum for phytoplankton, S is the CDM spectral “slope”

parameter, and n parameterizes the spectral variation of the particle backscattering. The difficulty in developing these models is the sensitivity of retrievals to choices of the parameters in the models ($a_{\text{ph}}^*(\lambda)$, S , and n ; Garver & Siegel, 1997; O'Reilly et al., 1998). In the GSM01 model, these parameter values have been optimized for global applications by using an extended version of the SeaBAM data set (Maritorena et al., 2002). A global optimization procedure determined the “best” values of $a_{\text{ph}}^*(\lambda)$, S , and n , for retrieving the three unknowns— C , $a_{\text{cdm}}(443)$, and $b_{\text{bp}}(443)$. Details concerning the GSM01 model and its global tuning can be found in Maritorena et al. (2002). The GSM01 water reflectance model can then be represented functionally as,

$$\hat{\rho}_w(\lambda) = \hat{\rho}_w(\lambda; C, a_{\text{cdm}}(443), b_{\text{bp}}(443)). \quad (7)$$

Note that $\rho_w(\lambda)$ is assumed to be independent of illumination or viewing geometry and that henceforth, a circumflex will indicate a modeled quantity.

The GSM01 model has the advantage that it is a function only of wavelength and the three retrieved products. This makes it straightforward to implement in the SOA procedure. Carder et al. (1999) use essentially the same decomposition of absorption and scattering coefficients; however, their expression for $b_{\text{bp}}(\lambda)$ contains parameters that are dependent upon reflectance itself. This makes the model difficult to implement in the present procedure. It is important to note that the GSM01 model is tuned to essentially the same data set as the O'Reilly et al. (1998) bio-optical algorithms and when tested with in situ data performs identically as the standard empirical algorithm used in processing SeaWiFS imagery (Maritorena et al., 2002). Hence, the GSM01 and the standard SeaWiFS processing should result in the same chlorophyll a concentration given the same $\rho_w(\lambda)$ estimates. This enables us to assess the SOA retrievals of C using standard SeaWiFS-data products.

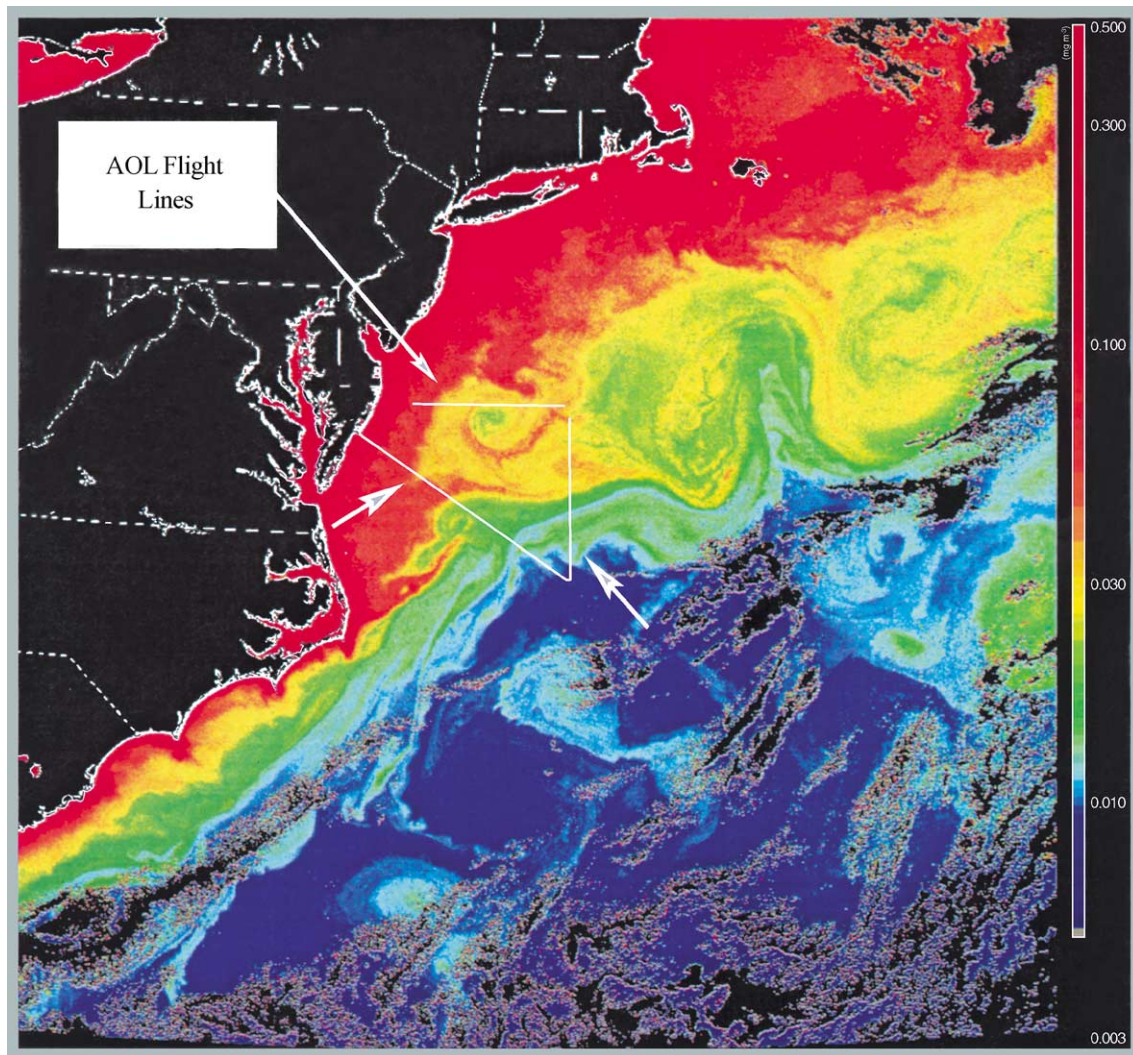


Fig. 1. $a_{\text{cdm}}(443)$ retrieved from the SeaWiFS image for day 279 of 1997 in the Middle Atlantic Bight. “Surface truth” data were obtained with the AOL along the white lines off the coast between the Chesapeake Bay and Delaware Bay. The color scale is logarithmic (labels are 0.003, 0.010, 0.030, 0.100, 0.300, and 0.500 m^{-1}).

5. The optimization procedure

The coupling of the atmosphere and ocean reflectance models is achieved as follows. The Rayleigh contribution $\rho_r(\lambda)$ is first subtracted from $\rho_t(\lambda)$ for each SeaWiFS band. One is then left with

$$\rho_{Aw}(G, \lambda, \text{measured}) \equiv \rho_A(G, \lambda) + t_v(G, \lambda)t_s(G, \lambda)\rho_w(\lambda). \quad (8)$$

The modeled counterpart of ρ_{Aw} can be expressed as

$$\begin{aligned} \hat{\rho}_{Aw}(G, \lambda, m_r, m_i, v, \tau_a, C, a_{\text{cdm}}(443), b_b(443)) \\ \equiv \hat{\rho}_A(G, \lambda, m_r, m_i, v, \tau_a) + \hat{t}_v(G, \lambda, m_r, m_i, v, \tau_a) \\ \times \hat{t}_s(G, \lambda, m_r, m_i, v, \tau_a) \times \hat{\rho}_w(\lambda, C, a_{\text{cdm}}(443), b_{\text{bp}}(443)). \end{aligned} \quad (9)$$

We assume that the water-leaving reflectance in the 765- and 865-nm SeaWiFS bands is negligible, which allows the direct estimation of v and τ_a from determinations of

$\rho_{Aw}(765)$ and $\rho_{Aw}(865)$ (Chomko & Gordon, 2001). However, rather than using the method described by Chomko and Gordon (1998, 2001), wherein an average (over all m_r and m_i) value of v is estimated at each pixel, we require an exact fit to $\rho_A(765)$ and $\rho_A(865)$ for each (m_r, m_i) combination. This results in 12 values of v and τ_a , for which the functions $v = v(m_r, m_i)$ and $\tau_a = \tau_a(m_r, m_i)$ are established by interpolation (Fig. 1 in Chomko & Gordon, 1998 shows that for a given $\rho_A(765)$ and $\rho_A(865)$, the value of $v(m_r, m_i)$ can vary as much as ± 0.2 to ± 0.4 from the mean as m_r and m_i are varied). Thus, given the functions $v(m_r, m_i)$ and $\tau_a(m_r, m_i)$, we minimize the quantity

$$\sum_{\lambda_i} \{ \hat{\rho}_{Aw}(G, \lambda_i, m_r, m_i, v, \tau_a, C, a_{\text{cdm}}(443), b_{\text{bp}}(443)) - \rho_{Aw}(G, \lambda_i, \text{measured}) \}^2 \quad (10)$$

over the remaining six SeaWiFS bands using standard optimization techniques to find the other five parameters

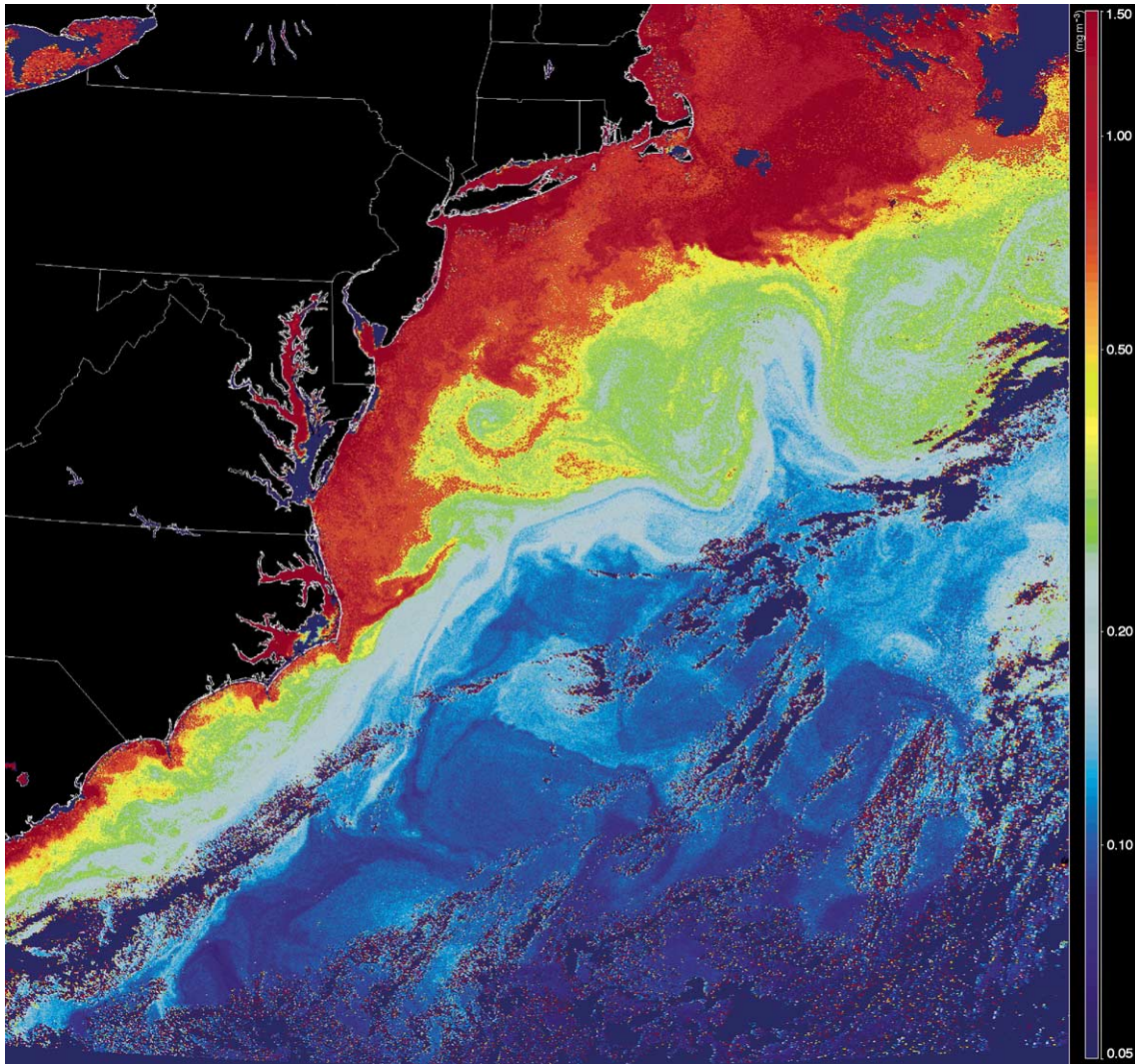


Fig. 2. C retrieved from SeaWiFS for the same image as Fig. 1. The color scale is logarithmic (labels are 0.05, 0.10, 0.30, 0.50, 1.00, and 1.50 mg m^{-3}).

to provide aerosol and ocean parameters simultaneously. In effect, we have optimized for seven parameters:

C , $a_{\text{cdm}}(443)$, $b_{\text{bp}}(443)$, v , τ_a , m_r , and m_i ;

using the eight spectral bands of SeaWiFS and the constraint that $\hat{\rho}_{\text{Aw}} = \rho_{\text{Aw}}$ exactly in the NIR. In the optimization, $\hat{\rho}_{\text{A}}(G, \lambda, m_r, m_i, v, \tau_a)$ is interpolated over the 72 grid (model) points. For interpolation in the m_i direction, we interpolate on $m_i^{1/4}$ rather than m_i itself as $\hat{\rho}_{\text{A}}(G, \lambda, m_r, m_i, v, \tau_a)$ is closer to linearity as a function of $m_i^{1/4}$. No interpolation is required for $\rho_w(\lambda)$ as an analytic formulation is used.

6. Application to SeaWiFS imagery

We applied the SOA algorithm to a full resolution SeaWiFS image from the Middle Atlantic Bight (MAB) acquired on day 279 of 1997. As described in Chomko and Gordon (2001), the atmosphere over the MAB on this day was quite turbid with $\tau_a(865)$ exceeding 0.2 over significant

portions of the image. Retrieved images of $a_{\text{cdm}}(443)$, C , and $b_{\text{bp}}(443)$ are shown in Figs. 1, 2, and 3, respectively. As expected, strong gradients of $a_{\text{cdm}}(443)$ and C are observed across the Gulf Stream. Near the coast, values of $a_{\text{cdm}}(443)$ and C , respectively, are more than 100 and 10 times greater than values found within the Sargasso Sea. The front for $a_{\text{cdm}}(443)$ found across the Gulf Stream is particularly strong. Retrievals of $a_{\text{cdm}}(443)$ are especially high near known river outflows as is expected (Hoge, Vodacek, Swift, Yungel, & Blough, 1995; Vodacek, Blough, DeGrandpre, Peltzer, & Nelson, 1997; Degrandpre, Vodacek, Nelson, Bruce, and Blough, 1996). Series of mesoscale meander and ring features as well as many smaller, sub-mesoscale features are also observed on either side of the Gulf Stream in both $a_{\text{cdm}}(443)$ and C . High values of C ($>1.5 \text{ mg m}^{-3}$) are found associated with Georges Bank, while retrievals of $a_{\text{cdm}}(443)$ there do not increase as intensely.

Contrasting this, values of $b_{\text{bp}}(443)$ show considerably weaker patterns associated with the Gulf Stream and its associated features (Fig. 3). High values of $b_{\text{bp}}(443)$ are

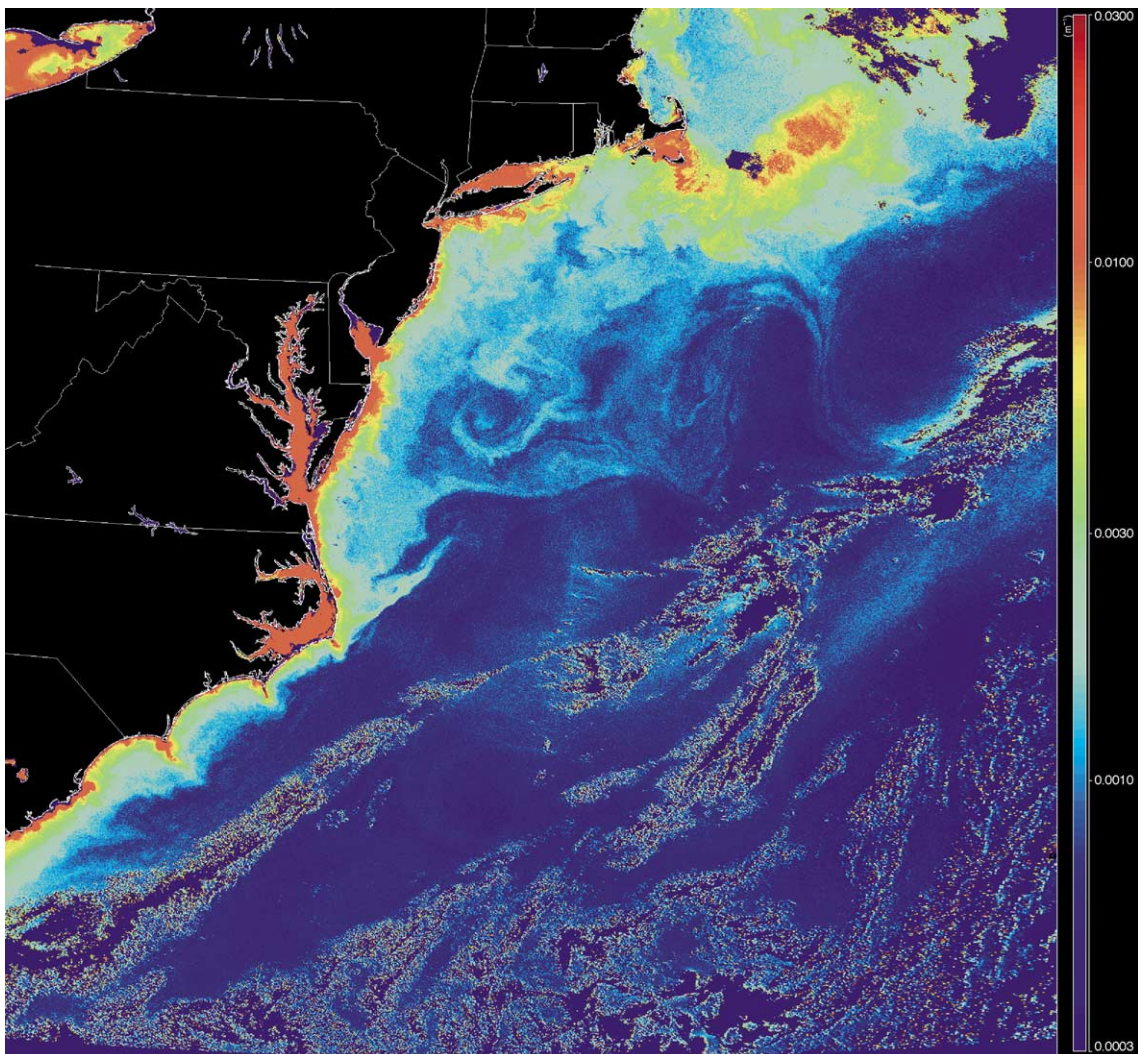


Fig. 3. $b_{\text{bp}}(443)$ retrieved from SeaWiFS for the same image as Fig. 1. The color scale is logarithmic (labels are 0.0003, 0.0010, 0.0030, 0.0100, and 0.0300 m^{-1}).

associated with enclosed, semi-enclosed, and near-shore waters, particularly for locations where intense values of $a_{\text{cdm}}(443)$ and C are found, such as Georges Bank. Ocean variations in the value of $b_{\text{bp}}(443)$ are relatively small, typically a factor of 2–3 across the Gulf Stream.

7. CDM validation using Airborne Lidar

Superimposed on the image of $a_{\text{cdm}}(443)$ are three tracks flown by the Airborne Oceanographic Lidar (AOL) on the same day, providing an independent estimate of surface ocean optical properties. Laser-induced fluorescence returns from the AOL can be used to derive the absorption co-

efficient at 355 nm, $a_{\text{CDOM}}(355)$, of chromophoric dissolved organic matter (CDOM)—the dissolved component of CDM (e.g., Hoge et al., 1995). This technique is based upon an empirical relationship between the fluorescence of CDOM, excited by a laser operating at 355 nm, and the absorption coefficient of CDOM at 355 nm (Hoge, Vodacek, & Blough, 1993). Because the SOA retrieves $a_{\text{cdm}}(443)$, to compare the two we must either convert the retrieved value to that at 355 nm or the AOL value to 443 nm. We chose the latter.

The AOL-determined value of $a_{\text{cdm}}(443)$ is derived from its measurement of $a_{\text{CDOM}}(355)$ through multiplication by the factor, $\exp(-S(443 - 355))$. Using the value of S from GSM01 ($S=0.0206 \text{ nm}^{-1}$), Fig. 4a compares the SOA-retrieved $a_{\text{cdm}}(443)$ with the AOL-retrieved dissolved com-

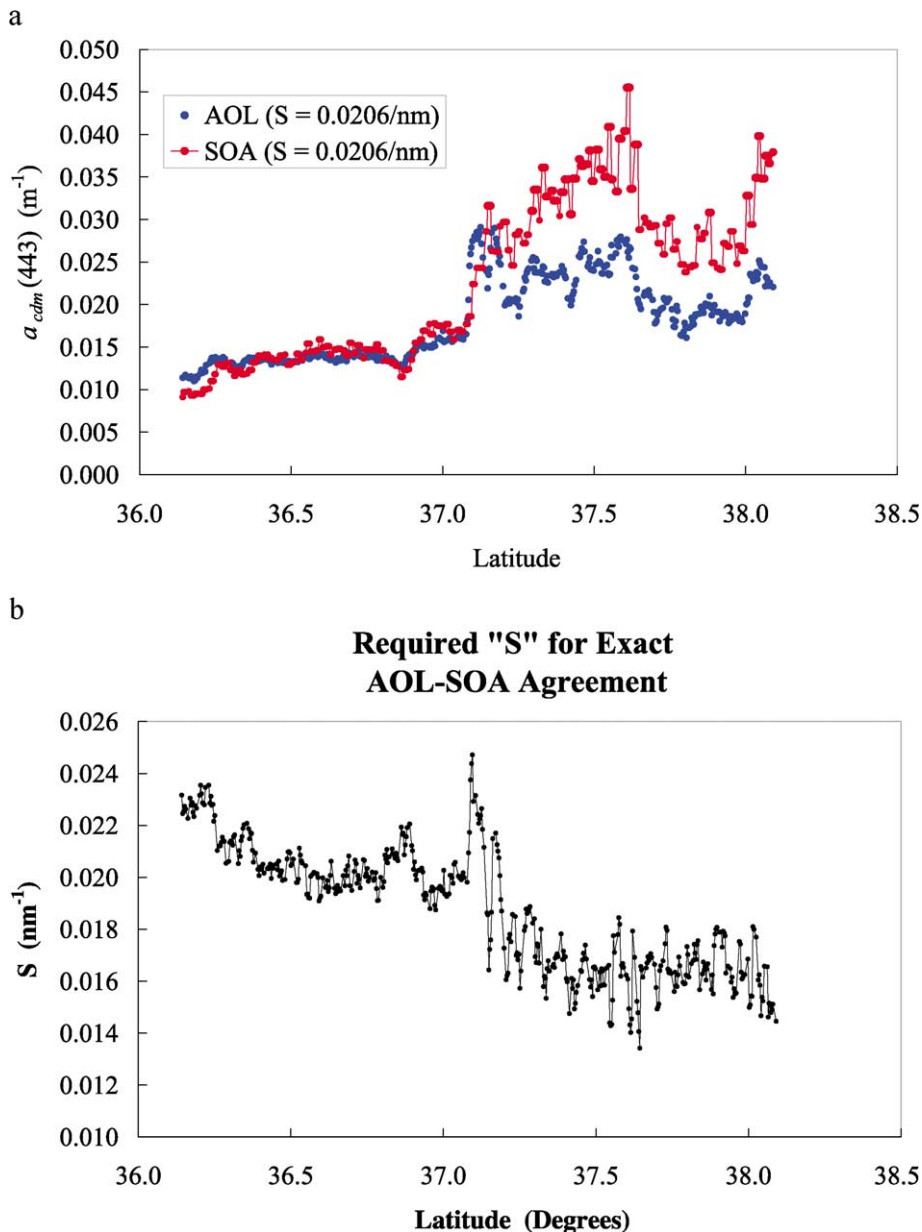


Fig. 4. (a) $a_{\text{cdm}}(443)$ derived from the AOL and the SOA along the north–south AOL flight line in Fig. 1. (b) Value of S required to bring the AOL-retrieved $a_{\text{CDOM}}(443)$ into agreement with the SOA-retrieved $a_{\text{cdm}}(443)$ for the north–south track in Fig. 1.

ponent $a_{\text{CDOM}}(443)$ from the north–south AOL transect shown in Fig. 1. We see that there is excellent agreement between the two estimates in and south of the Gulf Stream. Even the small-scale variations in the AOL measurements of $a_{\text{CDOM}}(443)$ are captured by the SOA retrievals. However, this agreement is degraded to the north where the SOA values are always larger than the AOL. Besides the possibility of measurement/algorithm error, there may be two physical reasons for the disagreement. First, across the entire transect, a single value for S (0.0206 nm^{-1}) was used to convert the AOL-retrieved dissolved component at 335–443 nm. Such a value may be characteristic of oligotrophic waters of the Gulf Stream; however, coastal waters with significant terrestrial exchanges are characterized by lower S values for the CDOM spectrum (e.g., Blough & DelVecchio, 2002; Green & Blough, 1994). Second, the SOA retrieves the absorption of *both* the dissolved and suspended detrital components, while the AOL retrieves just the dissolved component. Therefore, in the absence of measurement or model error, the AOL estimate should always be smaller than the SOA retrieval. However, for most oceanic environments, detrital particulates make only small contributions to the $a_{\text{cdm}}(443)$ signal (Siegel et al., 2002). An extensive data set of spectrophotometric absorption measurements from the

Gulf of Maine and Georges Bank shows $a_{\text{dp}}(443)$ to be 17.2% (s.d. = 12.9%, $N=403$) of the observed $a_{\text{cdm}}(443)$ value (Siegel et al., 2001). Field observations from the shelf regions around Florida and the Bahamas Islands indicate that detrital particles only contribute 12.4% of the $a_{\text{cdm}}(443)$ value (s.d. = 9.0%, $N=272$). Thus, $a_{\text{dp}}(443)a_{\text{CDOM}}(443)$, so $a_{\text{cdm}}(443) \approx a_{\text{CDOM}}(443)$.

It is interesting to determine the value of S required to bring the SOA retrieved $a_{\text{cdm}}(443)$ into confluence with the AOL-retrieved $a_{\text{CDOM}}(443)$ at each point along the track (Fig. 4b). The resulting S values show a clear trend of decreasing into the mesotrophic waters as would be expected (Green & Blough, 1994). Similar results are found for the other two tracks.

Assuming that $a_{\text{CDOM}}(443)$ is the major component of the satellite-retrieved $a_{\text{cdm}}(443)$, these comparisons suggest that the SOA is performing well in retrieving $a_{\text{cdm}}(443)$ from the SeaWiFS imagery. The spatial patterns of their variation are well matched, and there is reasonable quantitative agreement. Differences in the two are readily explained by differences in the S value associated with the CDOM source. This result also suggests that indices for land–ocean interaction can be developed from retrievals of the S value with a new generation of ocean

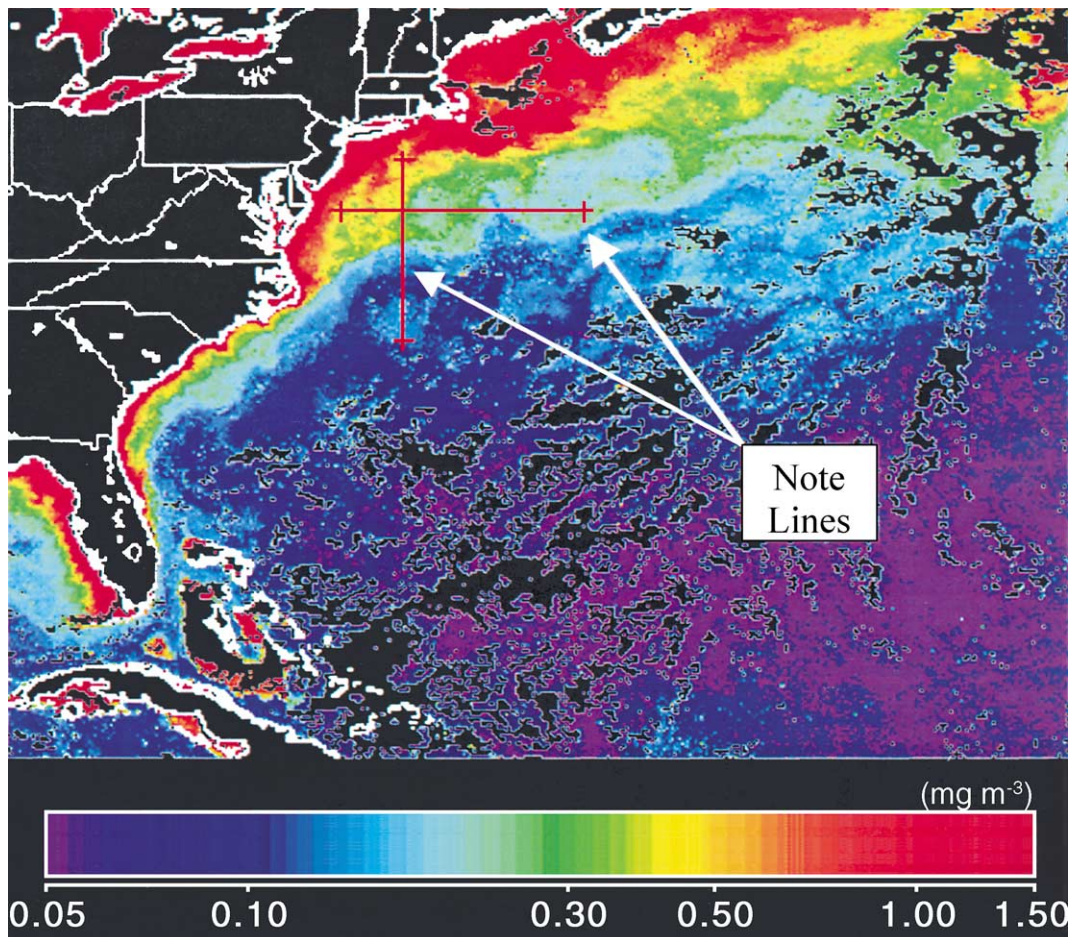


Fig. 5. SeaWiFS 8-day mean C for days 273–280 1997. Extractions in Fig. 6 are along the red lines on the figure.

color sensors, e.g., equipped with spectral bands in the UV.

8. Chlorophyll validation using SeaWiFS operational products

To examine the quality of the chlorophyll *a* retrieval, we compared it to the standard SeaWiFS product (STD). The SeaWiFS data have been validated (Hooker & McClain, 2000) and we take them to be surface truth for the comparison. We used the SeaWiFS 8-day mean (days 273–280) covering the image we examined (day 279). The chlorophyll *a* composite image is presented in Fig. 5.

Fig. 6 compares the 8-day mean with the SOA-retrieved values of *C* along the two lines drawn in Fig. 5. There is close agreement between the mean STD processing for the 8-day period and the SOA for day 279, suggesting that the SOA also performs well in retrieving *C*.

Fig. 6 also suggests a difficulty with the SOA algorithm for regions characterized by large values of $a_{\text{cdm}}(443)$, e.g., greater than about $0.05\text{--}0.10\text{ m}^{-1}$. For these regions, the SOA algorithm often gives $C \approx 0.7\text{ mg/m}^3$. In our operation of the optimization algorithm, we use four sets of starting values for the five parameters. Optimization proceeds with each and after 10 iterations, the starting point that produced the smallest residual is allowed to continue until the convergence criteria are meant, or until further iterations are

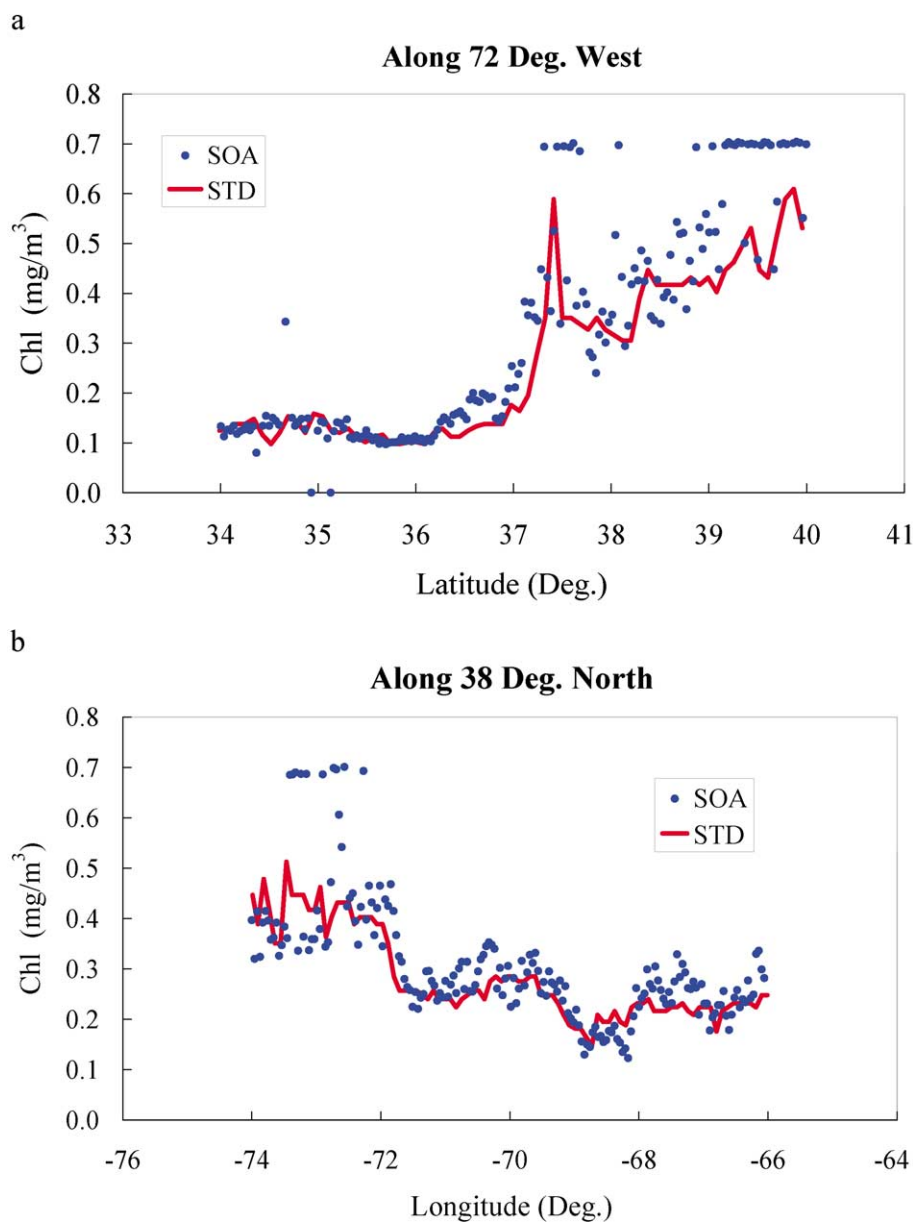


Fig. 6. Comparison between the SeaWiFS standard 8-day *C* (STD) and that derived by the SOA. Data are extracted along the lines in Fig. 5: (a) north–south line; (b) east–west line.

deemed to result in little gain. The chlorophyll *a* value for two of the starting points is 0.7 mg m^{-3} . Thus, it appears that for high $a_{\text{cdm}}(443)$ environments, the SOA gets “stuck” near its starting point. We are trying to find a way to circumvent this behavior; however, it may be that for high- $a_{\text{cdm}}(443)$ and high-*C* regions, it is not possible to estimate *C* accurately using the present SOA procedure because ρ_w in the blue becomes too small.

9. Aerosol parameters

Retrieved values of the aerosol single scattering albedo (ω_0) are seen to be nearly unity over most of the image (Fig. 7). This contrasts the previous Chomko and Gordon (2001) application of the SOA procedure where retrieved ω_0 values were unity (non-absorbing aerosol) over the low-*C* areas south of the Gulf Stream and ~ 0.95 in the higher-*C* regions. The difference here is the use of the GSM01 vs.

the Gordon et al. (1988) reflectance model. Values of ω_0 are far from unity only very close to the coast (Fig. 7). There, the water-leaving reflectance in the NIR is not negligible (Case 2 waters; Gordon & Morel, 1983; Siegel et al., 2000). This suggests that the SOA has achieved its goal of a nearly complete decoupling of $\rho_A(\lambda)$ and $\rho_w(\lambda)$. As mentioned earlier, in the Chomko and Gordon (2001) application, it was found that when the SOA was applied to imagery for which the aerosol concentration was very low, $\rho_A(\lambda)$ and $\rho_w(\lambda)$ did not totally decouple as evidenced by the presence of strong oceanic patterns in ω_0 . In Fig. 8, we present the image of ω_0 retrieved for Middle Atlantic Bight from SeaWiFS imagery acquired on day 281 of 1997. Day 281 of 1997 was the very clear day examined in Chomko and Gordon (2001). Fig. 8 shows $\omega_0 \sim$ unity over the whole region, with only a faint suggestion of oceanic features, except in the coastal regions. In contrast, the inserted image, which is processed by replacing the GSM01 reflectance model with the Gordon et al. reflectance model, clearly

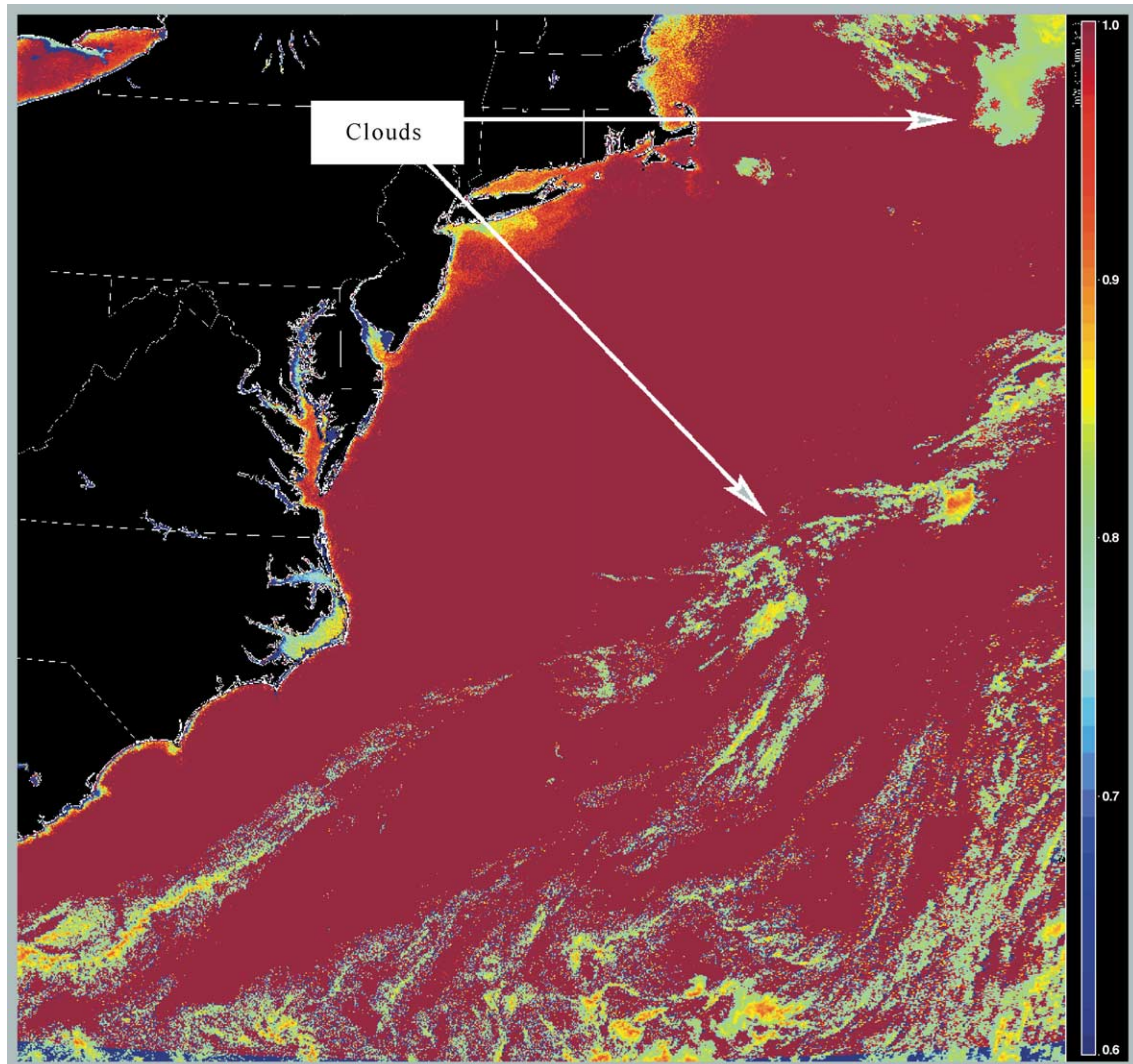


Fig. 7. Retrieved ω_0 for day 279.

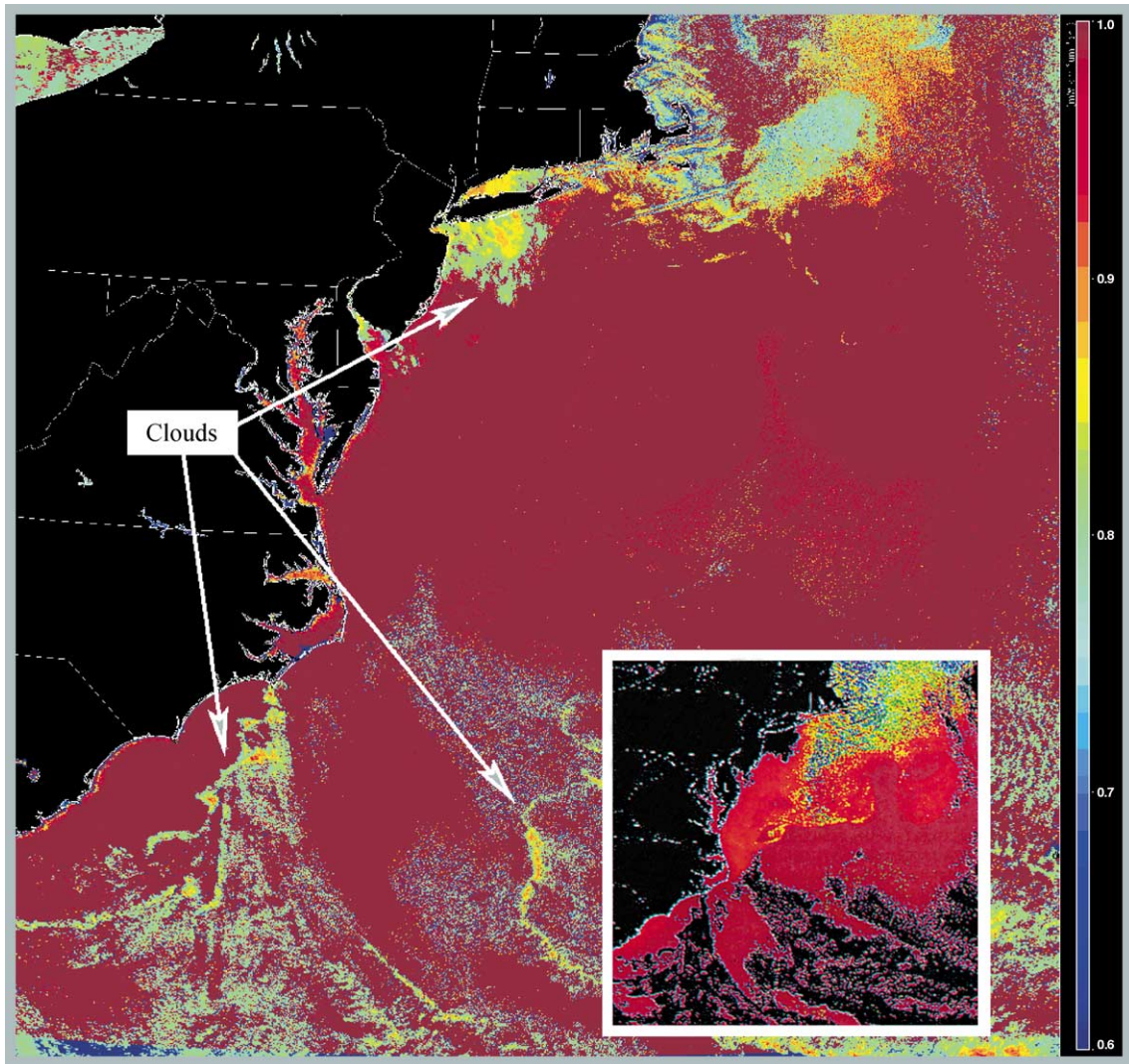


Fig. 8. Retrieved ω_0 for day 281. Full image uses the methodology described in the text. Inserted image is also the retrieved ω_0 , but with GSM01 ρ_w model replaced by the Gordon et al. (1988) ρ_w model. Note that the inserted image retrieves lower ω_0 values and shows obvious oceanic structure in ω_0 in the slope and shelf waters. This indicates that there is incorrect atmospheric correction in these regions. In contrast, oceanic features are nearly absent from the full image, indicating a better decoupling between the oceanic and atmospheric reflectances (color bar labels are 0.6, 0.7, 0.8, 0.9, and 1.0.)

shows oceanic features north of the Gulf Stream. This failure to decouple $\rho_A(\lambda)$ and $\rho_w(\lambda)$ in the inserted image is due to the incomplete nature of the Gordon et al. model for $\rho_w(\lambda)$. In the present application (using GSM01), lowering $\rho_w(412)$ relative to $\rho_w(443)$ can be achieved by either increasing $a_{\text{cdm}}(443)$ or m_i . When using Gordon et al., this is possible *only* by increasing m_i (which decreases ω_0). We note that even with GSM01, there are still coastal regions (including Georges Bank) where low values of ω_0 are retrieved. These are in Case 2 waters for which the GSM01 parameters (e.g., S , $a_{\text{ph}}^*(\lambda)$, and/or n) are not properly optimized.

10. Concluding remarks

We have applied the SOA to SeaWiFS imagery using a more complete model to provide $\rho_w(\lambda)$ for the optimization

procedure. Validation with airborne (AOL) and space-borne (SeaWiFS) acquired surface “truth,” and a nearly complete decoupling of $\rho_A(\lambda)$ and $\rho_w(\lambda)$ suggests that the algorithm is a useful alternative to processing ocean color imagery. It should have wide applicability in that it works well in the presence of non-absorbing aerosols and has the potential to provide accurate retrievals in cases where the aerosol is strongly absorbing, e.g., urban pollution. However, the present coupled algorithm will not work well for mineral dust aerosols because of the assumed wavelength-independent refractive index.

More importantly, the extension of the algorithm to Case 2 waters is immediate. The principal difficulty in Case 2 waters is that one can no longer assume $\rho_w \approx 0$ in the NIR (e.g., Ruddick et al., 2000; Siegel et al., 2000). Thus, direct application of the algorithm in its present form would yield incorrect results for $v(m_r, m_i)$ and $\tau_a(m_r, m_i)$. However, given

a bio-optical model for $\rho_w(\lambda)$ tuned to the particular Case 2 waters of interest (needed to interpret $\rho_w(\lambda)$ anyway) that extends into the NIR, one can perform an additional iteration to improve $v(m_r, m_i)$ and $\tau_a(m_r, m_i)$ in the following manner. First, apply the SOA with $\rho_w = 0$ in the NIR and find values for all of the parameters. Next, use the water parameters to predict ρ_w in the NIR and remove its contribution to $\rho_t - \rho_r$ in the NIR. Operate the $v - \tau_a$ portion of the algorithm to obtain a better estimate for $v(m_r, m_i)$ and $\tau_a(m_r, m_i)$. Finally, operate the visible portion of the optimization to obtain improved water parameters, etc. Although such an approach is computationally intensive, Case 2 water regions for which a particular bio-optical algorithm would be applicable are usually not spatially large, so intense computation is not an obstacle to processing Case 2 water regions. Such an extension is not effected here because the GSM01 model is not (yet) tuned for turbid Case 2 waters.

Acknowledgements

This research was supported by NASA Contracts NAS5-31363 (HRG), NAS5-31734 (HRG), NAS5-0096 (SM), NAS5-99083 (DAS), and NAG5-9818 (DAS). The authors would like to thank the SeaWiFS Project (Code 970.2) and the Distributed Active Archive Center (Code 902) at the Goddard Space Flight Center, Greenbelt, MD 20771, for the production and distribution of these data, respectively. These activities are sponsored by NASA's Earth Science Enterprise Program. Finally, we extend our thanks to the NASA Airborne Oceanographic Lidar Team for providing the CDOM measurements, and to the reviewers for helpful suggestions.

References

- Andre, J.-M., & Morel, A. (1991). Atmospheric corrections and interpretation of marine radiances in CZCS imagery, revisited. *Oceanologica Acta*, 14, 3–22.
- Blough, N. V., & Del Vecchio, R. (2002). Chromophoric DOM in the coastal environment. In D. A. Hansell, & C. A. Carlson (Eds.), *Biogeochemistry of marine dissolved organic matter* (pp. 509–546). San Diego, CA: Academic Press.
- Bricaud, A., & Morel, A. (1987). Atmospheric corrections and interpretation of marine radiances in CZCS imagery: use of a reflectance model. *Oceanologica Acta*, 7, 33–50.
- Carder, K. L., Chen, F. R., Lee, Z. P., Haws, S. K., & Kamykowski, D. (1999). Semianalytical moderate resolution imaging spectrometer algorithms for chlorophyll *a* and absorption with bio-optical domains based on nitrate-depletion temperatures. *Journal of Geophysical Research*, 104C, 5403–5421.
- Chomko, R. M., & Gordon, H. R. (1998). Atmospheric correction of ocean color imagery: use of the Junge power-law aerosol size distribution with variable refractive index to handle aerosol absorption. *Applied Optics*, 37, 5560–5572.
- Chomko, R. M., & Gordon, H. R. (2001). Atmospheric correction of ocean color imagery: test of the spectral optimization algorithm with SeaWiFS. *Applied Optics*, 40, 2973–2984.
- Degrandpre, M. D., Vodacek, A., Nelson, R. K., Bruce, E. J., & Blough, N. V. (1996). Seasonal seawater optical properties of the US Middle Atlantic Bight. *Journal of Geophysical Research*, 101C, 22727–22736.
- Garver, S., & Siegel, D. (1997). Inherent optical property inversion of ocean color spectra and its biogeochemical interpretation: 1 time series from the Sargasso Sea. *Geophysical Research*, 102C, 18607–18625.
- Gordon, H. R., Brown, O. B., Evans, R. E., Brown, J. W., Smith, R. C., Baker, K. S., & Clark, D. K. (1988). A semi-analytical radiance model of ocean color. *Journal of Geophysical Research*, 93D, 10909–10924.
- Gordon, H. R., Clark, D. K., Mueller, J. L., & Hovis, W. A. (1980). Phytoplankton pigments derived from the Nimbus-7 CZCS: initial comparisons with surface measurements. *Science*, 210, 63–66.
- Gordon, H. R., Du, T., & Zhang, T. (1997). Remote sensing ocean color and aerosol properties: resolving the issue of aerosol absorption. *Applied Optics*, 36, 8670–8684.
- Gordon, H. R., & Morel, A. Y. (1983). Remote assessment of ocean color for interpretation of satellite visible imagery: a review. New York: Springer-Verlag, 114 pp.
- Green, S. A., & Blough, N. V. (1994). Optical absorption and fluorescence properties of chromophoric dissolved organic matter in natural waters. *Limnology and Oceanography*, 39, 1903–1916.
- Hoge, F. E., & Lyon, P. E. (1996). Satellite retrieval of inherent optical properties by linear matrix inversion of oceanic radiance models—an analysis of model and radiance measurement errors. *Journal of Geophysical Research*, 101C, 16631–16648.
- Hoge, F. E., Vodacek, A., & Blough, N. V. (1993). Inherent optical properties of the ocean: retrieval of the absorption coefficient of chromophoric dissolved organic matter from fluorescence measurements. *Limnology and Oceanography*, 38, 1394–1402.
- Hoge, F. E., Vodacek, A., Swift, R. N., Yungel, J. K., & Blough, N. V. (1995). Inherent optical properties of the ocean: retrieval of the absorption coefficient of chromophoric dissolved organic matter from airborne laser spectral fluorescence measurements. *Applied Optics*, 34, 7032–7038.
- Hooker, S. B., Esaias, W. E., Feldman, G. C., Gregg, W. W., & McClain, C. R. (1992). *An Overview of SeaWiFS and Ocean Color; SeaWiFS Technical Report Series, vol. 1*. In S. B. Hooker, & E. R. Firestone (Eds.), NASA, Greenbelt, MD, Technical Memorandum 104566, July 1992.
- Hooker, S. B., & McClain, C. R. (2000). The calibration and validation of SeaWiFS data. *Progress in Oceanography*, 45, 427–465.
- Hovis, W. A., Clark, D. K., Anderson, F., Austin, R. W., Wilson, W. H., Baker, E. T., Ball, D., Gordon, H. R., Mueller, J. L., El Sayed, S. Y., Sturm, B., Wrigely, R. C., & Yentsch, C. S. (1980). Nimbus-7 Coastal Zone color scanner: system description and initial imagery. *Science*, 210, 60–63.
- Lee, Z. P., Carder, K. L., Hawes, S. K., Steward, R. G., Peacock, T. G., & Davis, C. O. (1994). Model for the interpretation of hyperspectral remote-sensing reflectance. *Applied Optics*, 33, 5721–5732.
- Maritorena, S., Siegel, D. A., & Peterson, A. R. (2002). Optimization of semi-analytical ocean color model for global scale applications. *Applied Optics*, 41, 2705–2714.
- Moulin, C., Gordon, H. R., Banzon, V. F., & Evans, R. H. (2001). Assessment of Saharan dust absorption in the visible from SeaWiFS imagery. *Journal of Geophysical Research*, 106D, 18239–18249.
- Moulin, C., Gordon, H. R., Chomko, R. M., Banzon, V. F., & Evans, R. H. (2001). Atmospheric correction of ocean color imagery through thick layers of Saharan dust. *Geophysical Research Letters*, 28, 5–8.
- O'Reilly, J. E., Maritorena, S., Mitchell, B. G., Siegel, D. A., Carder, K. L., Garver, S. A., Kahru, M., & McClain, C. (1998). Ocean color chlorophyll algorithms for SeaWiFS. *Journal of Geophysical Research*, 103C, 24937–24953.
- Roesler, C. S., & Perry, M. J. (1995). In situ phytoplankton absorption, fluorescence emission, and particulate backscattering spectra determined from reflectance. *Journal of Geophysical Research*, 100, 13279–13294.
- Ruddick, K. G., Ovidio, F., & Rijkeboer, M. (2000). Atmospheric correction of SeaWiFS imagery for turbid coastal and inland waters. *Applied Optics*, 39, 897–912.

- Siegel, D. A., Maritorena, S., Nelson, N. B., Hansell, D. A., & Lorenzi-Kayser, M. (2002). Global ocean distribution of colored dissolved and detrital materials. *Journal of Geophysical Research* (in press).
- Siegel, D. A., Wang, M., Maritorena, S., & Robinson, W. (2000). Atmospheric correction of satellite ocean color imagery: the black pixel assumption. *Applied Optics*, 39, 3582–3591.
- Smith, R. C., & Wilson, W. H. (1981). Ship and satellite bio-optical research in the California Bight. In J. F. R. Gower (Ed.), *Oceanography from space* (pp. 281–294). New York: Plenum.
- Vodacek, A., Blough, N. V., DeGrandpre, M. D., Peltzer, E. T., & Nelson, R. K. (1997). Seasonal variation of CDOM and DOC in the Middle Atlantic Bight: terrestrial inputs and photooxidation. *Limnology and Oceanography*, 42, 674–686.
- Yang, H., & Gordon, H. R. (1997). Remote sensing of ocean color: assessment of the water-leaving radiance bidirectional effects on the atmospheric diffuse transmittance. *Applied Optics*, 36, 7887–7897.